Challenging Glass 5 – Conference on Architectural and Structural Applications of Glass
Belis, Bos & Louter (Eds.), Ghent University, June 2016.

ISBN 978-90-825-2680-6

Design and Engineering of a Dry Assembled Glass Block Pedestrian Bridge

A. Snijder [a], J. Smits [a], T. Bristogianni [b] & R. Nijsse [a, b]
[a] *TU Delft, Faculty of Architecture and the Built Environment, The Netherlands, a.h.snijder@tudelft.nl*
[b] *TU Delft, Faculty of Civil Engineering and Geosciences, The Netherlands*

Inspired by the glass masonry technique developed by the TU Delft Glass and Transparency Lab for the Crystal House in Amsterdam, a 14 meter span pedestrian bridge is envisioned, also consisting of cast glass elements. In contrast to the Crystal House project that employs an adhesively bonded glass block system, here dry assembly of the glass elements is proposed to allow for a demountable structure. To achieve this, a constant compression force is introduced in the bridge through its arch-shape. This compression force and a special interlocking geometry of the blocks will ensure the stability of the structure, like a medieval stone arch. The paper will discuss the exploratory design and engineering leading up to the construction of the first 3 meter span mock-up. This includes studies on the visual appearance of the bridge, studies on the glass block geometry, calculations on stresses in the glass elements, experiments on force transfer through dry-connected elements and mould design for casting of the complex geometries of the glass elements.

Keywords: Glass, cast glass, bridge, dry assembly

1. Introduction

This paper focuses on the preliminary design and engineering of a dry-assembled glass block pedestrian bridge. This 14m span bridge is planned to be constructed at the TU Delft campus and will mark the entrance to the "Green Village" innovation park. Its construction involves cast glass blocks which are dry-assembled in an arch shape. An artist's impression is given in Figure 1 and 28.

Fig. 1 Artist impression of the glass bridge

The built environment has seen a number of applications of glass block construction. The most common example is the hollow glass block (Murray, 2013 p. 77). Solid glass block construction has been applied in four notable projects so far. In the Atocha Memorial (Christoph & Knut, 2008), the Crown Fountain (Hannah, 2009), the Optical House (Hiroshi, 2012) and the Crystal House (MVRDV, 2015). See *'A completely transparent, adhesively bonded soda-lime glass block masonry system'* by F. Oikonomopoulou et al. for a more detailed description of these projects.

The successive projects show the tendency that the glass block construction is engineered to be more and more loadbearing. From the hollow glass blocks which are each individually supported, to the façade of the crystal house which bears its self-weight and lateral imposed loads. (Oikonomopoulou et al 2015).

The current glass bridge project, presented in this paper, builds on the experience of the preceding glass block façade project in which TU Delft was involved (Oikonomopoulou et al. 2016). In this paper an overview of the initial design considerations and engineering principles is provided.

2. Alternatives

2.1. Parameters

A number of parameters are set by the location or production method:

- The span of the bridge should be 14 meters.
- The bridge should be constructed from solid cast glass elements
- The cast glass elements should weigh no more than 12 kg to reduce annealing time. A tradeoff between requirements of structural depth for the bridge deck on the one hand, and a risk of the blocks becoming too slender on the other, resulted in the height for the block set at 350 mm.
- The elements should be easy to dis- and re- assemble.
- No chemical adhesives should be used.

Three alternatives were considered: 1) The arch, 2) The trussed beam, and 3) The post-tensioned beam.These options are selected because they introduce only compression in the glass elements.

Below a brief description of these three structural principles as they apply to the bridge is given and some rudimentary calculations show the maximum average stresses in the glass. For all principles a live load of 5 kN/m^2, a deadload of 0.35*25=8.75 kN/m^2 and a span of 14 m have been assumed. Since this is purely a comparative exercise safety factors were not considered. The calculation are done for a segment of the bridge with a width of 1 meter.

2.2. The arch

A circular arch (see figure 2) was considered with a radius so large that it approximates a catenary curve. The arch thus generates an axial compressive force and negligible bending due to its self weight. Uneven live loads result in bending, but the tensile stress resulting from this bending can be compensated for by that axial compressive stress.

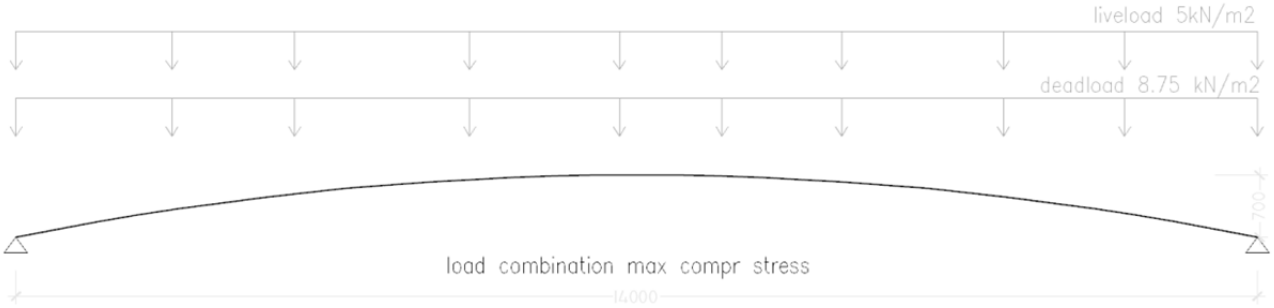

Fig. 2 The arch evenly loaded

lateral thrust of the arch: $H = \frac{\frac{1}{8}ql^2}{f} = \frac{\frac{1}{8}(8.75+5)*14^2}{0.7} = 481\ kN$

axial force: $N = \sqrt{(0.5ql_{arch})^2 + H^2} = \sqrt{(0.5 * 13.75 * 14.1)^2 + 481^2} = 491\ kN$

stress: $\sigma_n = \frac{491}{1*0.35} = 1402$ -> 1.4 N/mm^2

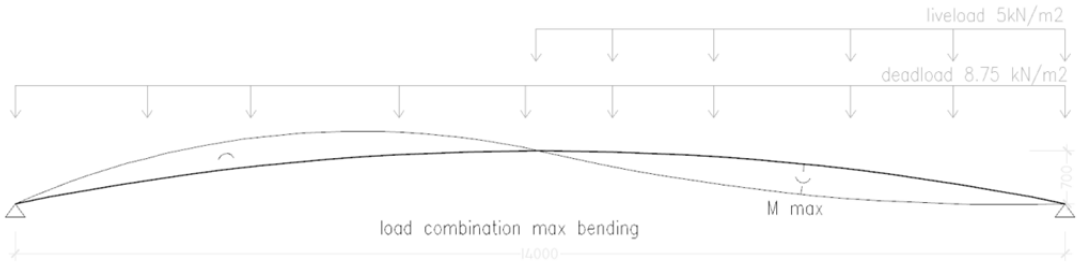

Fig. 3 The arch unevenly loaded

Lateral thrust of the arch: $H = \frac{q_{dead}l^2}{8f} + \frac{q_{live}l^2}{16f} = \frac{8.75*14^2}{8*0.7} + \frac{5*14^2}{16*0.7} = 394\ kN$

Max bending moment occurs at $\frac{3}{4}l$: $m_{3l/4} = \frac{1}{64}q_v l^2 = \frac{1}{64} * 5 * 14^2 = 15.31\ kNm$

Stress bending: $\sigma_m = \frac{m*z}{I} = \frac{15.31*0.175}{\frac{1}{12}*1*0.35^2} = 262$->0.262 N/mm^2

Axial force at $\frac{3}{4}l$: $N = \sqrt{\left(\frac{3}{16}q_l*l+\frac{1}{4}q_d*l\right)^2 + H^2} = \sqrt{\left(\frac{3*5*14}{16}+\frac{8.75*14}{4}\right)^2 + 394^2} = 396.5\ kN$

Compressive stress: $\sigma_n = \frac{396.5}{1*0.35} = 1132.9$ -> 1.13 N/mm^2

Netto stresses in section: 1.13+0.262=1.4 N/mm^2 and 1.13-0.262=0.87 N/mm^2. both compression.

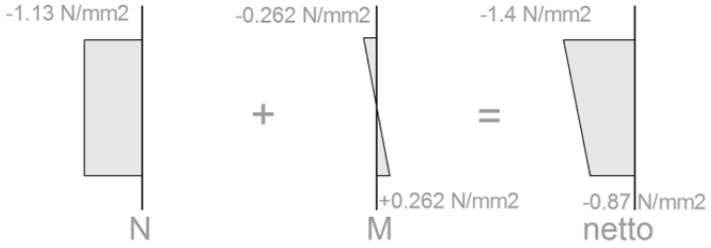

Fig. 4 Stress diagrams for the arch unevenly loaded.

2.3. The trussed beam

The trussed beam principle was considered as two steel cables spanned below the bridge deck with two spacers (see figure 5 below). The spacers act like supports for the bridge deck. They exert a vertical force on the cable, which in turn introduces a compressive horizontal force in the bridge deck. The deck spanning between the supports and spacers is activated in bending and generates tensile stress. This tensile stress can again be compensated by the compressive stress introduced in the deck by the cables. Distance f between bridge deck and cable determines the axial compressive stress in the bridge.

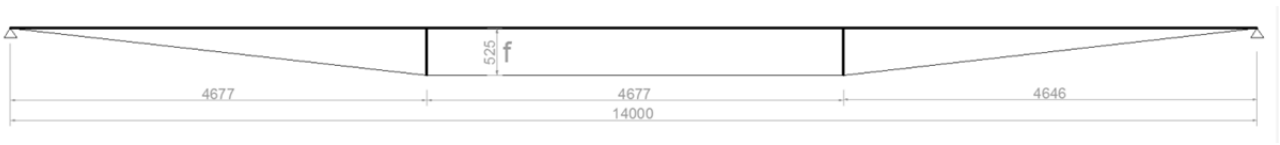

Fig. 5 The trussed beam principle

- bending stress: $\sigma_m = \frac{ql^2}{12*h^2}$
- axial prestress: $\sigma_n = \frac{ql^2}{8*f*h}$

For zero tensile stress ($\sigma_m = \sigma_n$) a distance f of 525mm is required.

The max stress in glass: $\sigma_n + \sigma_m = \frac{ql^2}{8*f*h} + \frac{ql^2}{12*h^2} = 3.7\ {}^{N}/_{mm^2}$

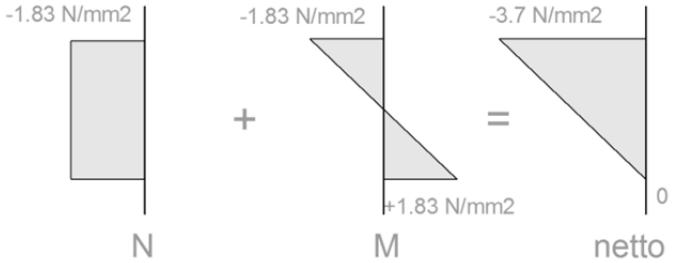

Fig. 6 Stress diagrams for the trussed beam

2.4. The post tensioned beam

A cable running through the bridge deck, fixed at both ends. It is tensioned so it will introduce a compressive force (F) in the bridge deck. The cable is fixed eccentrically to the ends of the beam by a distance of 1/6th of the height of the deck below the center line of the deck. This is done to also generate an upward bending moment that introduces more compressive stress in the lower flange of the bridge deck. Both the axial compressive force and the upward bending moment introduced by the cable can result in a big enough compressive stress to compensate for the tensile stress arising from bending due to vertical loading by dead and live loads.

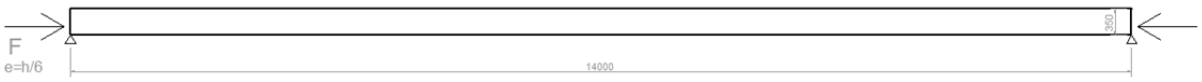

Fig. 7 The post tensioned beam

The axial stress from the post tensioning: $\sigma_n = \frac{F}{h}$

The bending stress from the h/6 eccentricity of the post tensioning: $\sigma_{m1} = \frac{F}{h}$

The bending stress from the dead and live load: $\sigma_{m2} = \frac{3ql^2}{4h^2}$

For no tensile stress ($\sigma_n + \sigma_{m1} = \sigma_{m2}$) a post tensioning force of F=2887.5 kN is required

Max stress in glass: $\sigma_n - \sigma_{m1} + \sigma_{m2} = 24.75\ N/mm^2$

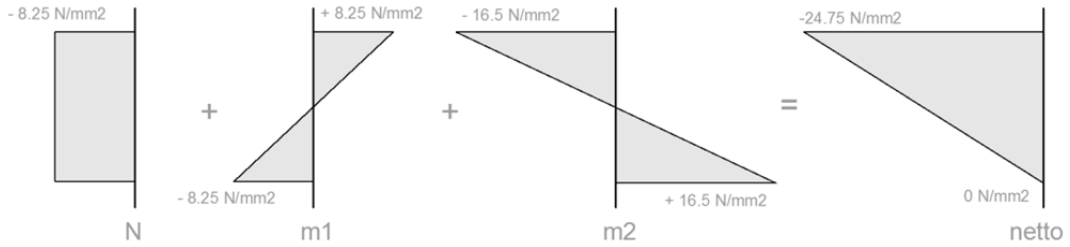

Fig. 8 Stress diagrams for the post tensioned beam

The arch is the favoured structural principle because 1) With the given height of 350 mm for the glass block it generates the lowest stresses (-1.4 N/mm^2) in the glass. 2) it is the only option that can be constructed out of glass with the least amount of extra other materials and 3) The design has the lowest number of unique components.

3. Shape exploration

3.1. Interlock

Dry assembly of the glass blocks was for the client, The Green Village, an important demand for sustainability reasons. Because glass has a low friction coefficient, an interlocking geometry had to be developed to allow for more shear force transfer between the blocks. A series of models were printed to further explore the shape of the interlock.

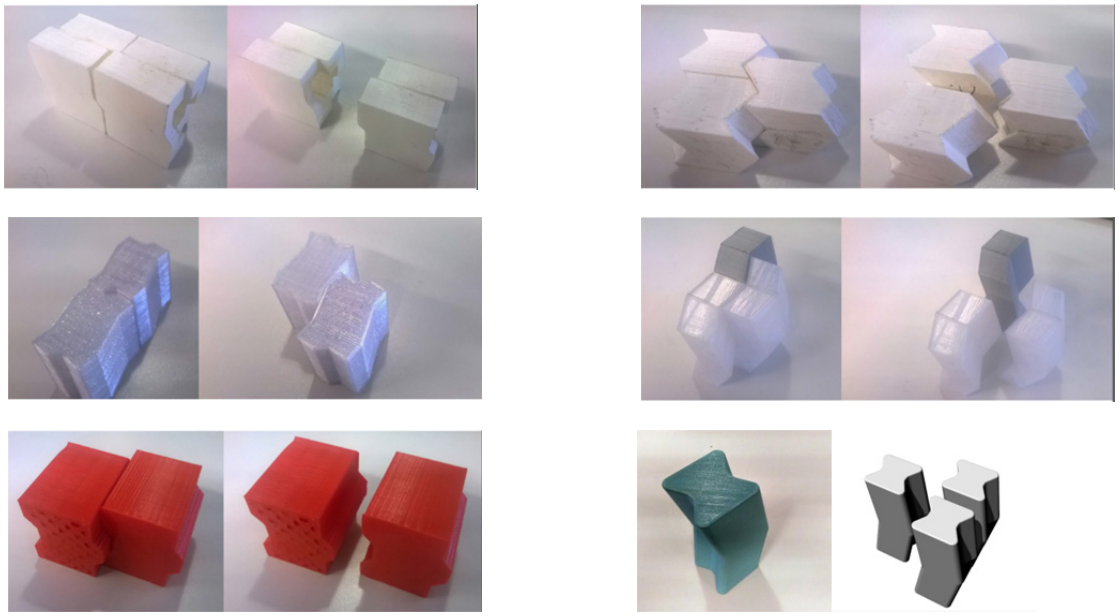

Fig. 9 Prototypes for shape exploration

Parallel to developing the shape of the brick for the purpose of structural interlocking, checks were done to asses if the shape could be effectively cast in glass. For this 3D printed moulds and sugar glass were used. Between 100 and 150 degrees Celsius sugar glass can become a similar viscosity to actual molten glass. After cooling sugar glass also shows, to some extent, brittle behaviour (Micciche, 2007). This allows for quick exploration of the flow of the glass in the mould.

It was observed that thick syrupy fluid like molten glass or sugar glass has trouble filling every corner of the mould. When corners are angular and sharp there is the risk of the corner not being completely filled by the glass. Also sharp corners in cast glass objects can be prone to chipping or cracking. This means that the bricks must have edges that are preferable obtuse and chamfered or rounded.

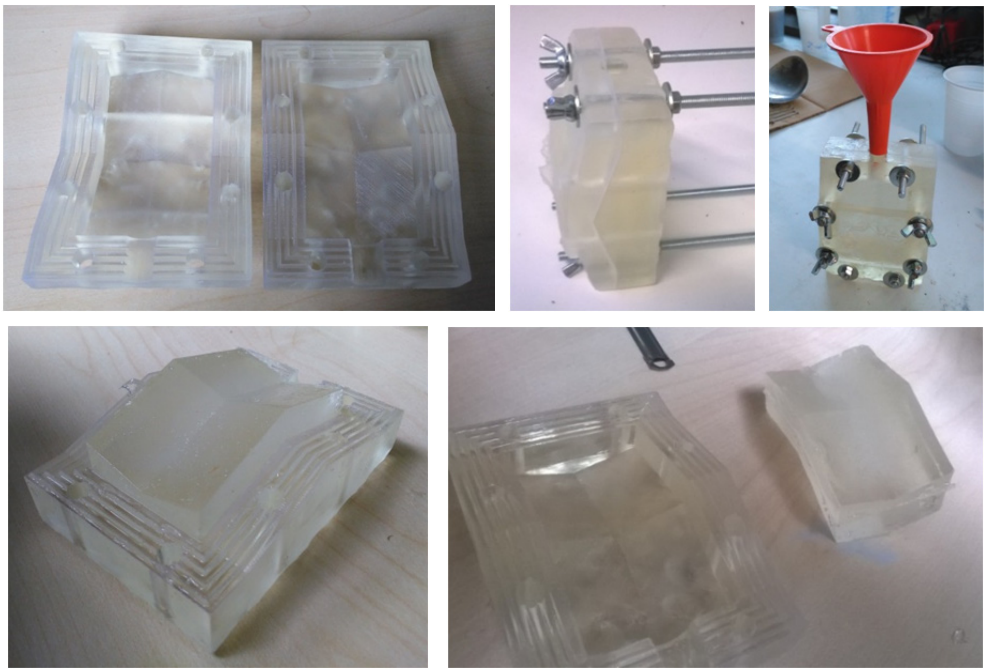

Fig. 10 3D printed moulds for exploratory casting experiments with sugar glass.

4. Indicative experiments

4.1. Glass on glass normal force transfer

An average compressive stress resulted from the analytical explorative calculations of no more than 1.4 N/mm^2. Although some authors claim a theoretical compressive strength of glass of over 200 N/mm^2, the strength of cast glass elements, as applied in the former glass block façade project, tends to be lower (around 20 N/mm^2) because of a bigger chance of imperfections in big volumes of glass (Oikonomopoulouet al, 2015). Since the average stresses in the bridge will likely be no higher than 1.4 N/mm^2, the strength of the glass itself is more than sufficient. However, the force transfer between the blocks could be critical if stress concentration occur due to an uneven contact surface.

To obtain insight in this phenomena some exploratory experiments were carried out. Two glass blocks were placed in a compression machine. The glass surfaces directly to the machine were cushioned with 4 mm rubber pads. The glass faces touching one another were either left clean, or sprinkled with sand of different grades of coarseness. The blocks were soda lime glass cast by Poesia in Italy.

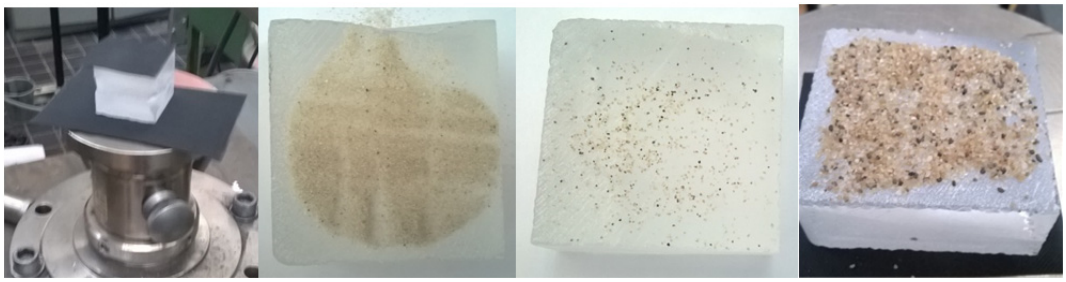

Fig. 11exploratory experiment with sand between contact surfaces of glass blocks; fine, medium and coarse

Table 1: results

Specimen	Grain size	Failure load F [kN]
4	No contamination	Over 100 kN (machine limit)
5	Medium	76.3
6	Coarse	96.8
7	Medium	96.4
9	Fine	95.6

The experiment was meant to be indicative and the test setup is not sufficiently controlled to draw any real conclusions. However, since none of the samples had contact surfaces of more than 80x80 mm we can tentatively conclude that an average stress of up to 10 N/mm^2 can be transferred in compression between two glass elements with granular inclusions at the interface or with uneven contact surfaces.

5. Interlocking geometries for bending and shear

Six different geometries (see figure 12) for the block to block interlock have been explored using mdf lasercut models. The arch relies on the interlock for transferring shear forces.

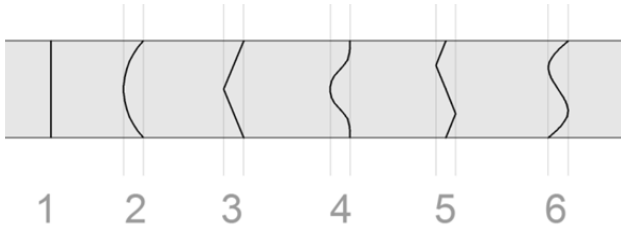

Fig. 12 Six different shapes for the block to block interlock

For assessing the structural behaviour of interface shape numbers 1 to 3 the model has been placed horizontally on a table. The blocks fit precisely between the supports. The end blocks are prevented from displacement by notches protruding into the support.

5.1. nr 1 - The flat surface

When a shear force is generated in the structure and very little bending (fig 13) it is observed that the block is easily moved. When the point load is placed in the middle, where it also generates a bending moment that compresses the block at the top, the block has increased resistance to sliding.

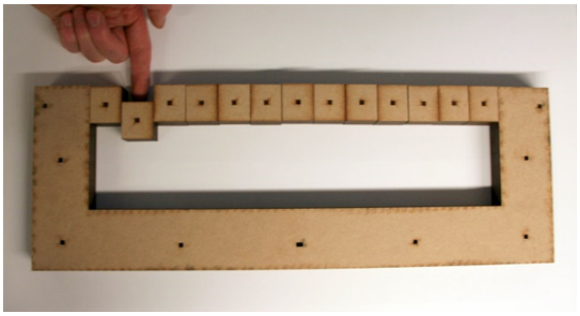

Fig. 13 Flat surface shear

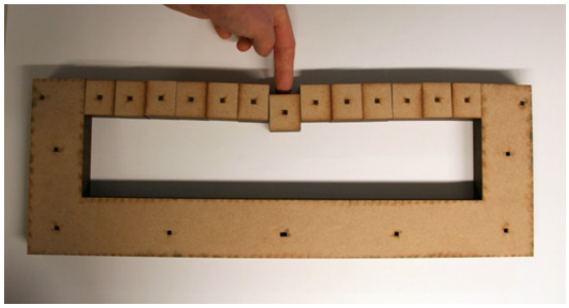

Fig. 14 Flat surface shear and bending.

5.2. nr2 - the bow

It can be observed that the curved line works as an interlock for transferring just shear. When the point load is applied in the middle of the span and bending is induced, it acts like a hinge and the span collapses. Where the flat surface interface was seen to withstand bending to some extent but not shear, the bow shows the opposite behaviour; it withstands shear but not bending.

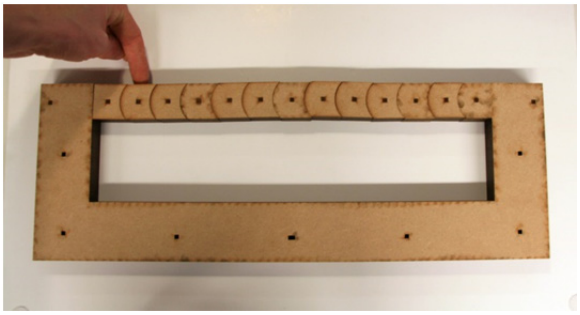

Fig. 15 Bow shear

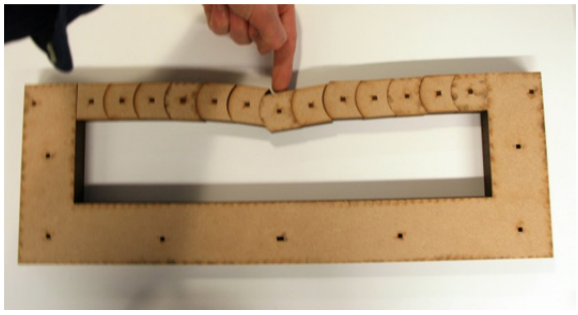

Fig. 16 Bow bending and shear

5.3. nr 3 - the kink

The kink resembles the behaviour of the bow, although the mismatch between the kink shape and a perfect bow shape seems to have as a result that the span generates more horizontal thrust when hinging, allowing it to withstand a larger load before collapsing.

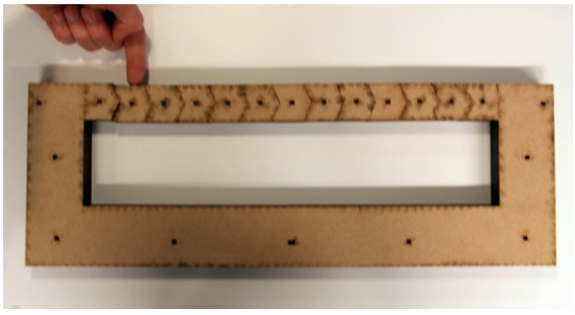

Fig. 17Kink shear.

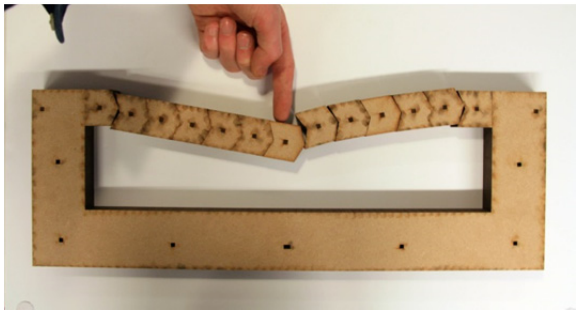

Fig. 18 Kink bending and shear

5.4. nr 4 - the belly, nr 5 – the lightning bolt and nr 6 – the snake

The last 3 options are much better both in shear and bending. To effectively compare their relative performance a more accurate experiment has been performed in the lab. The first three options were of such insufficient loadbearing capacity that they have been scrapped for further comparative study in the lab.

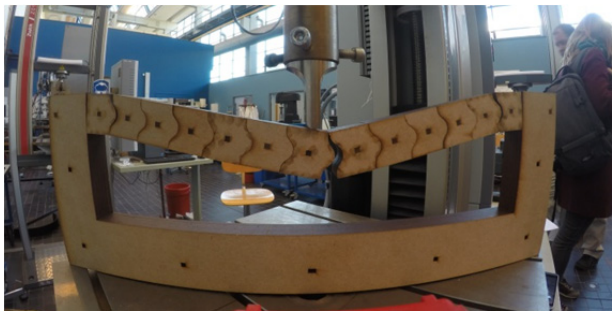

Fig. 19 Belly bending and shear

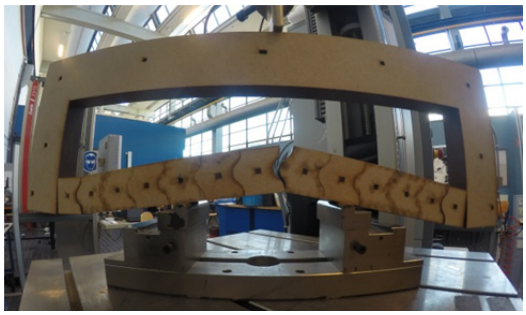

Fig. 20 Belly bending

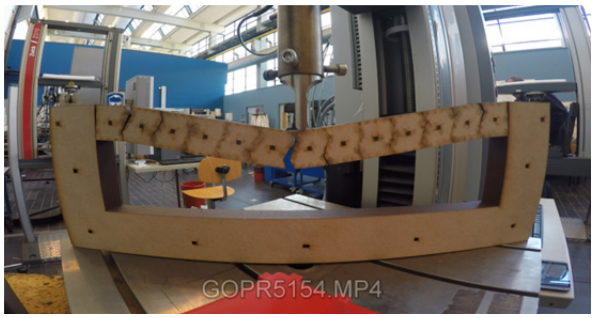

Fig. 21 lightning bending and shear

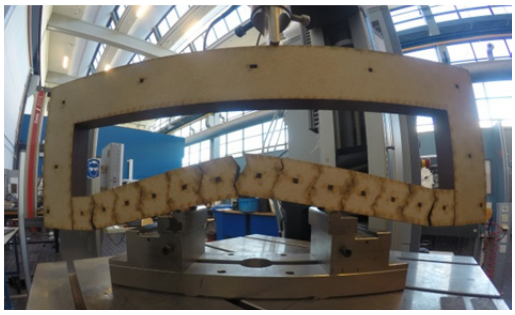

Fig. 22 Lightning bending

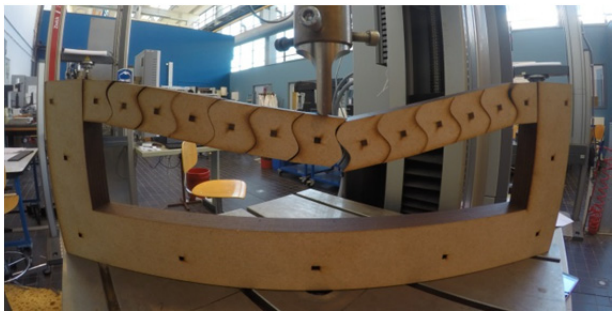

Fig. 23 Snake bending and shear

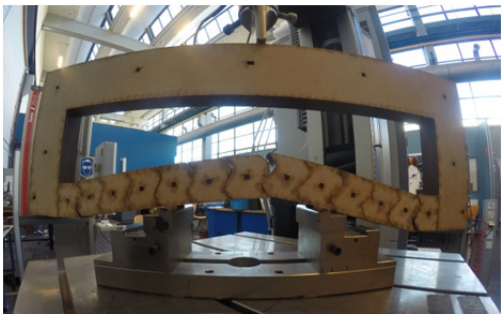

Fig. 24 Snake bending

3-Point and a 4 point bending tests were performed on the different block shapes to see the effect of shear and bending and of just bending without shear.

Table 2: results

Specimen	3 or 4 point bending	Failure load F [N]
Belly [3]	3	108
Belly [3]	4	110.2
Lightning [4]	3	96.0
Lightning [4]	4	124.5
Snake [5]	3	45.4
Snake [5]	4	55.9

The belly shape block interlock can be observed to show the highest failure load in the 3-point bending tests. For the four point bending test the lightning shape block interlock shows the highest failure load.

It can be observer in fig 26 that the snake shape block interlock starts behaving like a hinge again when the bending deformation has opened up the interface at the bottom. Just like observed with the bow shape this greatly diminishes the ability of the blocks to withstand bending, as it starts behaving like a mechanism with three hinges, rather than a static structure. The snake shape was drawn using a spline curve, instead of two half circles with equal radius like a yin yang (see fig 27). This reduces the tendency for the interlock to behave like a hinge to some extent. The lightning shape interlock is even further removed from the ideal constant radius of a hinge and exhibits a still higher failure load.

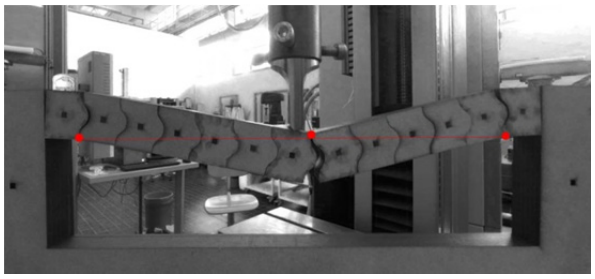

Fig. 25 Belly bending and shear

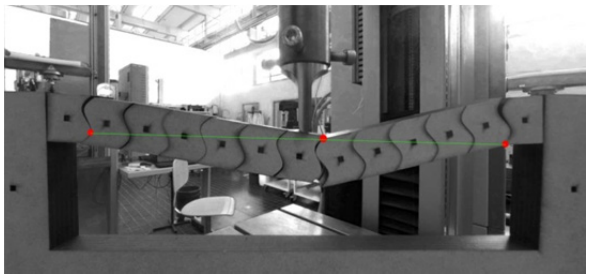

Fig. 26 Snake bending and shear

The belly shape block interlock has planar areas at its extremities. The images show that rotation happens around the top or bottom corner of the interface between the blocks. Figures 25 and 26 above show the bow shape blocks and the snake shape blocks during the 3 point bending tests. These were the last frames from the time-lapse before the snap-through collapse happened. The (explosive) collapse seems to occur when the middle hinge passes below the line that connects the support hinges. For the snake shape block the picture seems to indicate that rotation happens not necessarily around a point at the very bottom of the interface (point b in fig 27 below) but rather at point r, where the shear force and normal force can be transferred from blow to block as well. This higher position of the hinge could explain the lesser performance of the snake block in 3 point bending.

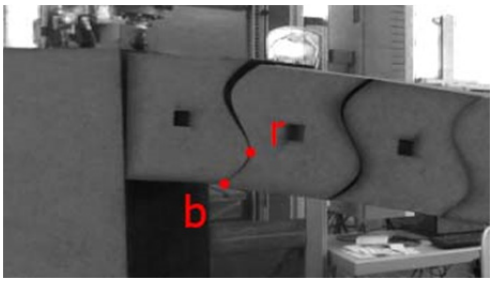

Fig. 27 Centres of rotation for the snake interface

6. Summary

For now the belly shaped block is favoured in terms of structural behavior as well as suitability for glass casting. The preliminary tests indicated that the belly shape was best able to resist the combination of shear and bending. The shape is also the only block (other than a regular flat one) that has no angles smaller than 90 degrees, which is favourable for the casting process.

Fig. 28 Artist impression of the bridge.

References

Christoph, P., & Knut, G. (2008). Innovative Glass Joints – The 11 March Memorial in Madrid. Paper presented at the Challenging Glass: Conference on Architectural and Structural Applications of Glass, Delft, The Netherlands.

Micciche, F., Leeuwen, van, P.B., Heisteeg, van der, C.L., Dill, F.B.C., Schmets, A.J.M., Lumley, R.N. (2007). First investigations into the autonomous recovery of structural damage in sugar-based glasses. Paper presented at the First International conference on self-healing materials. Noordwijkaan Zee, The Netherlands.

Murray, S. (2013). Translucent building skins: Material innovations in modern and contemporary architecture. London: Routledge.

Oikonomopoulou, F. Veer, F. Nijsse, R. Baardolf, K. A completely transparent, adhesively bonded soda-lime glass block masonry system. Journal of Facade Design and Engineering 2 (2014) p.201-221. IOS press, Amsterdam, the Netherlands.